Multiscale finite volume method for finite-volume-based simulation of poroelasticity

Sokolova, Irina; Bastisya, Muhammad Gusti; Hajibeygi, Hadi

DOI
10.1016/j.jcp.2018.11.039

Publication date
2019

Document Version
Accepted author manuscript

Published in
Journal of Computational Physics

Multiscale finite volume method for finite-volume-based simulation of poroelasticity

Irina Sokolova[a], Muhammad Gusti Bastisya[a], Hadi Hajibeygi[a,*]

[a]*Faculty of Civil Engineering and Geosciences, Department of Geoscience and Engineering, Delft University of Technology, Delft, The Netherlands*

Abstract

We propose a multiscale finite volume method (MSFV) for simulation of coupled flow-deformation in heterogeneous porous media under elastic deformation (i.e., poroelastic model). The fine-scale fully resolved system of equations is obtained based on a conservative finite-volume method in which the displacement and pore pressure unknowns are located in a staggered configuration. The coupling is treated through a fully-coupled fully-implicit formulation. On this fully-coupled finite-volume system, coarse-scale grids for flow and deformation are imposed. Local basis functions for scalar pore pressure and vectorial displacement unknowns are then solved over their respective local domains at the beginning of the simulation, and reused for the rest of the time-dependent simulations. These local basis functions are then clustered to form the prolongation operator. As for the finite-volume nature of the proposed multiscale system, finite-volume restriction operators for poroelastic systems are utilised. Once the coarse-scale system is solved, its solution is prolonged back to the original fine-scale resolution, providing approximate fine-scale solution. The finite-volume multiscale formulation provides conservative stress and mass flux both at fine and coarse scale. Several numerical test cases are provided first to validate the fine-scale finite-volume discrete fully-implicit simulation, and then to investigate the accuracy of the proposed multiscale formulation. Moreover we compare our fully implicit MSFV method with hybrid multiscale Finite Element-Finite Volume (h-MSFE-FV). Our multiscale method allows for quantification of the elastic geomechanical behaviour with using only a fraction of the fine-scale grid cells, even for highly heterogeneous time-dependent models. As such, it casts a promising approach for field-scale quantification of the mechanical deformation and stress field due to injection and production in a subsurface formation.

Keywords: Multiscale finite-volume method, poromechanics, geomechanics, porous media, finite volume method, Algebraic multiscale solver.

1. Introduction

Simulation of fluid flow and mechanical deformation in subsurface geological formations is challenging, since it involves large-scale models with highly heterogeneous coefficients and complex coupled fluid-rock interactions. Simulation accuracy is crucial for proper prediction of subsurface fluid dynamics and rock mechanics (stress and deformation), as well as safety assessments of the engineering applications (e.g., hydrocarbon and geo-thermal production). Note that subsurface flow and mechanics are coupled, and affect each other through effective stress and mass accumulation, according to the Biot theory [1].

The demand for accurate simulations urges the use of high-resolution models to capture both mechanical (i.e., elastic moduli) and hydraulic (i.e., permeability) properties. While the accuracy depends on resolving the highly heterogeneous coefficients with the physics-based coupled system of equations, high-resolution simulations of such

*Corresponding author.
Email addresses: i.v.sokolova@student.tudelft.nl (Irina Sokolova), MuhammadGustiBastisya@student.tudelft.nl (Muhammad Gusti Bastisya), h.hajibeygi@tudelft.nl (Hadi Hajibeygi)

systems are often impractical due to their computational cost. As such, computational efficiency depends on development of advanced simulation techniques which are (1) amenable for massive parallel processing, and, at the same time, (2) allow for accurate model order reduction (i.e., construct accurate (multilevel) coarse systems).

Classically, finite volume (FV) schemes have been the methods of choice for simulation of flow and transport [2], whereas finite-element (FE) methods have been preferred for mechanical deformation [3]. There exist several examples in the literature where conservative extensions of finite-element (FE) methods (e.g., mixed-FE) have been used for flow and transport simulations (e.g., see [4, 5]), as well as mechanical deformation [6]. Similarly, finite-difference [7] and FV methods have been proposed recently for mechanical deformation [8–10], motivated by their locally-conservative discrete stress representations with only 1 degree-of-freedom (DOF) per element. These FV methods for poromechanics are developed for sequentially-coupled flow-mechanics [10, 11], which depend on a careful treatment of the flow-mechanics coupling terms [12–17]. Fully-coupled approaches would add to the computational complexity, though they would naturally extend the stability of the simulation (compared with sequential approaches). Of particular interest is to develop an efficient and scalable fully-implicit flow-deformation system which would benefit from both enhanced stability and computational efficiency.

Irrespective of the type of the discretisation scheme and the choice of the coupling, the fine-scale highly resolved systems are required to be solved with advanced methods which are scalable for real-field applications. The multiscale finite-volume (MsFV) [18–22] and finite-element (MsFE) [23–26] methods are developed to provide accurate coarse-scale quantities when the underlying fine-scale system entails highly heterogeneous coefficients [27–32]. These methods allow for aggressive coarsening, via locally-solved basis functions, and have been so far extensively developed for flow and transport with complex fluid physics, from static 2-level multiscale sequential [33–35] to dynamic multi-level fully implicit systems [36–38]. Recently, a multiscale finite-element method was developed based on a FE fine-scale system for elastic deformation [39–41].

In this work, we develop a fully-implicit multiscale finite volume method for fully-coupled FV-based poromechanical formulation under the linear elastic deformation. The governing equations are discretised by employing a finite-volume scheme for both flow and mechanics in a fully coupled staggered-grid approach. This fully-coupled approach, compared with the sequential approaches, extends the stability of our simulations and generates a convenient framework for the cases with strong flow-deformation coupling terms. On this fully coupled locally conservative stress-mass system, multiscale coarse grids are imposed. Local basis functions for both flow (pore pressure) and deformation vector are solved, subject to local boundary conditions. The finite-volume coarse scale system is then constructed and solved in a finite-volume framework, using these local basis functions. The coarse-scale solution is interpolated back to the original fine-scale resolution, providing a good-approximate fine-scale solution. Through several homogeneous and heterogeneous time-dependent test cases, we first demonstrate the 2nd order of accuracy of our fully-coupled finite-scale discrete FV poromechanics formulation, and then the accuracy of our multiscale method for time-dependent scenarios. To provide a more thorough study, the accuracy of the MSFV solutions is also compared against the multiscale hybrid-FE-FV method.

Our brief paper is organised as follows. In section 2, the governing equations are briefly described. Then, the fully-coupled fine-scale finite-volume discrete system is presented in section 3. Subsequently, the multiscale finite-volume method is developed in section 4. Numerical experiments are then demonstrated in section 5, first to validate the consistency of our fully-coupled FV formulation, and then to investigate the performance of MSFV method. Finally, in section 6, the concluding remarks are given.

2. Governing equations

We consider a single-phase flow of slightly compressible fluid through deformable porous media. Subsurface rock is modelled based on linear elastic behaviour assumption with no gravity effect. The coupling of mechanical deformation and fluid pressure is modelled based on Biot's theory [1]. Under linear poroelasticity assumption, the domain Ω with external boundary Γ is considered. The set of governing equations for conservation of mass and linear momentum reads

$$\boldsymbol{\nabla} \cdot (C_{dr} : \boldsymbol{\nabla}^s \bar{u} - bpI) = f \tag{1}$$

and

$$b\nabla\cdot\dot{\bar{u}} + \frac{1}{M_b}\dot{p} - \nabla\cdot(\lambda\cdot\nabla p) = q, \tag{2}$$

respectively. Here, $\bar{u}$ and p are displacement vector and pore pressure, respectively, C_{dr} is drained elasticity tensor, M_b is the Biot's modulus, and b is Biot's coefficient. Moreover, $\lambda = \frac{K}{\mu}$ is the mobility, where K is rock permeability tensor and μ is fluid viscosity. Note that ∇^s is the symmetric gradient operator, and $\dot{p}$ and $\dot{\bar{u}}$ represent the time partial derivatives of p and $\bar{u}$. The linear elasticity constitutive law relates the effective stress to strain through

$$\sigma = C_{dr} : \nabla^s\bar{u}. \tag{3}$$

Equations (1) and (2) subject to the proper selection of the following general boundary conditions

$$\text{Prescribed boundary displacement:} \quad \bar{u}_\Gamma = \bar{u} \tag{4a}$$
$$\text{Prescribed boundary stress:} \quad (C_{dr} : \nabla^s\bar{u} - bpI)\cdot\bar{n} = \bar{f} \tag{4b}$$
$$\text{Prescribed boundary pore pressure:} \quad p_\Gamma = p \tag{4c}$$
$$\text{Prescribed boundary flux:} \quad -(\lambda\cdot\nabla p)\cdot\bar{n} = q \tag{4d}$$
$$\text{Initial pressure:} \quad p_\Omega = p_\Omega(t=0) \tag{4e}$$
$$\text{Initial displacment:} \quad \bar{u}_\Omega = \bar{u}_\Omega(t=0) \tag{4f}$$

form a well-posed system of equations for the vector of displacement $\bar{u}$ and pressure p as the unknowns.

3. Fine-scale formulation and simulation strategy

This section presents the fully-coupled FV formulation for poroelastic simulation. Similar as in the literature [10, 39, 41], the continuous displacement and pressure solutions are described according to their fine-scale nodal values and fine-scale basis (shape) functions. To do so, first the displacement and pressure unknowns are placed on a staggered grid as shown in Fig. 1. Both pressure and stress have a control volume (CV) assigned as for the FV nature

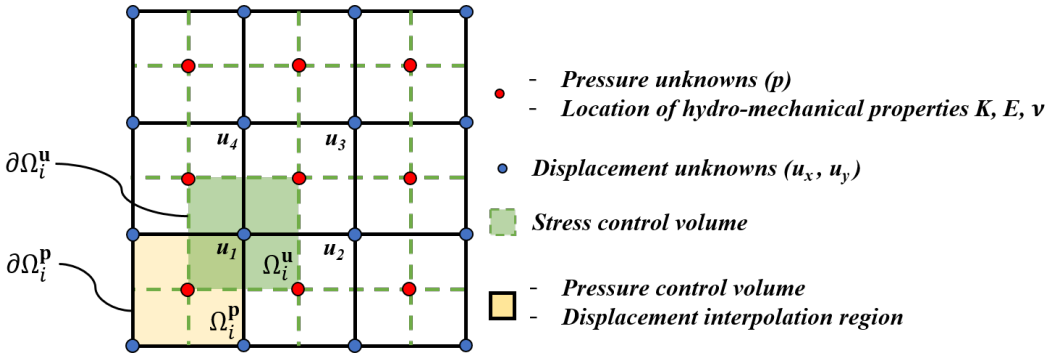

Figure 1: Fine-scale FV discretization grid. Pressure control volumes are denoted by solid black lines; dashed green lines correspond to stress control volume boundaries. Displacement interpolation regions coincide with pressure control volumes. Pressure unknowns are placed at fine-scale cell centeres, whereas displacement unknowns are located at the nodes. Permeability and elastic moduli are defined at the fine-scale cell centres.

of the discretisation [10]. Especially for our fully coupled extension for heterogeneous models, such configuration allows for the same data structure of permeability and elastic properties which generates a convenient framework to treat the subsurface heterogeneity.

In order to obtain a conservative numerical solution for displacement, linear momentum balance equation is integrated over stress control volumes Ω_i^u, i.e.,

$$\int_{\Omega_i^{\mathbf{u}}} \nabla\cdot(C_{dr} : \nabla^s\bar{u} - bpI)\, dV = \int_{\Omega_i^{\mathbf{u}}} f\, dV. \tag{5}$$

The left hand side (LHS) can be rewritten as a surface integral, using the divergence theorem, i.e.,

$$\int_{\partial\Omega_i^{\mathbf{u}}} (C_{dr} : \boldsymbol{\nabla}^s \bar{u}) \cdot \bar{n}\, dS - b \left(\int_{\partial\Omega_i^{\mathbf{u}}} p\, dS \right) I = \int_{\Omega_i^{\mathbf{u}}} f dV. \tag{6}$$

Note that if weighted integrals over element volumes are imposed, and is replaced by a weak formulation, a finite element discrete system is obtained [39]. In the LHS of Eq. (6), the first term corresponds to pure mechanical deformation (stress integral over closed surfaces), whereas the second term represents flow-deformation coupling (again, pressure integrated over closed surface).

Similarly, FV discrete system for flow is obtained by integrating the balance equation (2) over pressure control volume, i.e.,

$$b \int_{\Omega_i^{\mathbf{p}}} \boldsymbol{\nabla} \cdot \dot{\bar{u}}\, dV + \int_{\Omega_i^{\mathbf{p}}} \left(\frac{1}{M_b} \dot{p} - \boldsymbol{\nabla} \cdot (\lambda \cdot \boldsymbol{\nabla} p) \right) dV = \int_{\Omega_i^{\mathbf{p}}} q dV, \tag{7}$$

which is then re-written using divergence theorem as

$$b \int_{\partial\Omega_i^{\mathbf{p}}} \dot{\bar{u}} \cdot \bar{n}\, dS + \frac{1}{M_b} \int_{\Omega_i^{\mathbf{p}}} \dot{p}\, dV - \int_{\partial\Omega_i^{\mathbf{p}}} (\lambda \cdot \boldsymbol{\nabla} p) \cdot \bar{n}\, dS = \int_{\Omega_i^{\mathbf{p}}} q\, dV. \tag{8}$$

Note that the first term in LHS represents the dependency of the flow on the displacement field.

Similar to FE schemes, here in FV-based formulations one also needs to describe the continuum displacement and pressure field based on the nodal discrete values. For the displacement, one can write

$$\bar{u} \approx \sum_{i=1}^{4} \bar{u}_i\, N_i(x, y) \qquad \text{in} \quad \breve{\Omega}_i^{\mathbf{u}}, \tag{9}$$

where $\bar{u}_i$ are the displacement nodes (see Fig. 1) and $N_i(x, y)$ are the interpolation (shape) functions corresponding to each node of the element $\breve{\Omega}_i^{\mathbf{u}}$. Similar as in the literature [10, 39], we employ bilinear functions for displacement. This interpolation allows for convenient integration of the displacement and its derivatives over any interface, specially over finite-volume control volumes. Note that our finite volume formulation provides locally conservative stress field, with much fewer degrees of freedom compared with the mixed-FE formulation [6].

Similar formulation can be written for the pressure, which for the case of piece-wise constant approximation, reads

$$\bar{p} \approx p_i \qquad \text{in } \Omega_i^p. \tag{10}$$

Employing bilinear fine-scale interpolation for displacement and a classical (piece-wise constant) interpolation for pressure, allows computation of the FV integrals of the pressure and displacement unknowns. Note that for the convective flow term we follow a two-point-flux-approximation (TPFA) scheme.

The fully-implicit system of equation $\mathbf{A}\,\mathbf{x} = \mathbf{F}$, using Euler backward (implicit) time-integration, is finally obtained for the coupled displacement-pressure unknowns as

$$\underbrace{\begin{bmatrix} A_{uu} & A_{up} \\ A_{pu} & A_{pp} \end{bmatrix}}_{\mathbf{A}} \cdot \underbrace{\begin{bmatrix} \bar{u}^{n+1} \\ p^{n+1} \end{bmatrix}}_{\mathbf{x}} = \underbrace{\begin{bmatrix} \bar{F}_u \\ F_p \end{bmatrix}}_{\mathbf{F}}, \tag{11}$$

where $F_p = \bar{Q} + C p^n + A_{pu} \bar{u}^n$. The system matrix $\mathbf{A}$ is constructed by the finite-volume-based discrete entries for fluid and rock balance equations, $\mathbf{x}$ is the vector of the coupled unknowns, and $\mathbf{F}$ is the righ-hand-side vector containing source terms and explicitly known quantities. In addition, A_{uu} stands for stiffness matrix for pure mechanical deformation, A_{pp} corresponds to sum of transmissibility and accumulation matrices, A_{up} and A_{pu} represent flow-deformation and deformation-flow coupling terms, respectively, $\bar{F}_u$ and Q are stress and flow volumetric source terms. Moreover, t_n (and the index n) represents the previous time step, and C is the fluid mass accumulation matrix.

For the test cases presented in this paper, the solution of the fully-implicit system (11) is obtained by using the Matlab backslash (exact solver) operator. For large-scale test cases, iterative solvers need to be used for the solution of this system.

4. Multiscale formulation

The aim of multiscale method is to obtain an approximate fine-scale solution by using only a fraction of fine-scale cells. This is achieved by superimposing a coarse-scale grid on the fine-scale mesh, on which elastic and hydraulic properties are defined. The solution is obtained on a coarse scale via sets of local basis functions and interpolated back to the fine scale, using the same basis functions.

For fully coupled 2D poromechanics system solved on N_f fine-scale grid cells, there exist approximately $(3N_f)$ unknowns (1 pressure and 2 displacement per node). Thus, reducing the number of computational nodes would significantly reduce the size of matrix of linear system, and, consequently, improve the overall computational efficiency. In this work, a fully-coupled multiscale finite volume (MSFV) method is proposed for solving fully coupled poromechanics system. Independent coarse grids are superimposed on flow and deformation fine-scale mesh. In practice, this allows to apply a higher coarsening ratio to large geomechanics models, whereas flow can be solved with lower coarsening ratios if necessary.

The basis functions are obtained algebraically both for flow and mechanical deformation, in order to construct the prolongation operator and map the solution from coarse to fine scale. Restriction operators for flow and deformation, which map the fine-scale system to the coarse scale, are constructed in a finite volume manner as integration over the coarse control volumes.

4.1. Multiscale formulation for fully coupled poromechanics system

A multiscale formulation for fully coupled system of Eq. (11) requires construction of prolongation and restriction operators. Prolongation operator $\mathbf{P}$ transforms solution vector from coarse scale to fine scale, whereas restriction operator $\mathbf{R}$ brings quantities from fine to coarse scale. Thus, a coarse scale fully coupled poromechanics system for the coarse-scale unknowns $\mathbf{x_c} = (\bar{u}_c, p_c)^T$ and righ-hand-side $\mathbf{F_c} = \mathbf{R}\,(\bar{\mathbf{F}}_\mathbf{u}, \mathbf{F_p})^\mathbf{T} = \mathbf{R}\,\mathbf{F}$ yields

$$\mathbf{A_c}\,\mathbf{x_c} = (\mathbf{R}\,\mathbf{A}\,\mathbf{P})\,\mathbf{x_c} = \mathbf{F_c}. \tag{12}$$

In order to obtain a coupled coarse scale system (12) with independent coarsening ratios applied to pressure and displacement fields, global prolongation $\mathbf{P}$ and restriction $\mathbf{R}$ operators are constructed as

$$\mathbf{R} = \begin{bmatrix} \mathbf{R_u} & 0 \\ 0 & \mathbf{R_p} \end{bmatrix} \tag{13}$$

and

$$\mathbf{P} = \begin{bmatrix} \mathbf{P_u} & 0 \\ 0 & \mathbf{P_p} \end{bmatrix}, \tag{14}$$

where the sub-indexes $\mathbf{u}$ and $\mathbf{p}$ stand for sub-block operators for displacement and pressure, respectively. Note that the block-diagonal structure of the prolongation and restriction operators indicate the independent flow-mechanics local basis formulations. Once the coarse-scale system is solved, the approximate multiscale solution $\mathbf{x} \approx \mathbf{x}' = (\bar{u}', p')^T$ is found as

$$\begin{bmatrix} \bar{u}'^{n+1} \\ p'^{n+1} \end{bmatrix} = \mathbf{P} \begin{bmatrix} \bar{u}_c^{n+1} \\ p_c^{n+1} \end{bmatrix}. \tag{15}$$

Note that the MSFV simulation strategy can be improved by adopting an iterative procedure, which allows error control to any desired accuracy.

4.2. Construction of basis functions for mechanical deformation

The approximate fine-scale displacement $\bar{u}'$ is then obtained from the coarse-scale solution as

$$\bar{u}' = \mathbf{P_u}\bar{u}_c, \tag{16}$$

where prolongation operator $\mathbf{P_u}$ is constructed from displacement basis functions $\Phi_\mathbf{u}$ such that $\mathbf{P_u} = [\Phi_\mathbf{u}^1, ..., \Phi_\mathbf{u}^{N_\mathbf{u}^H}]$. Note that $N_\mathbf{u}^H$ is the number of coarse-scale displacement nodes. The displacement basis functions are computed by solving local momentum balance equation within primal coarse cells, subject to local boundary conditions as

$$\begin{cases} \nabla \cdot \left(C_{dr} : \nabla^s {\Phi_\mathbf{u}}_j^i \right) = 0 & in\ \Omega_j^P \\ \nabla_\parallel \cdot (C_{dr} : \nabla_\parallel^s {\Phi_\mathbf{u}}_j^i) = 0 & in\ \partial\Omega_j^P \\ {\Phi_\mathbf{u}}_j^i(\bar{x}_k) = \delta_{ik} & \forall\ \bar{x}_k \in \{1, ..., N_\mathbf{u}^H\}, \end{cases} \tag{17}$$

where ${\Phi_\mathbf{u}}_j^i$ stands for a basis function associated with coarse displacement node i in primal coarse block Ω_j^P, subscript $\parallel$ denotes a reduced problem along primal coarse cell boundary $\partial\Omega_j^P$ and δ_{ik} is the Kronecker delta. While the local basis functions are solved fully coupled, the localization condition, i.e., the reduced problems for both x- and y-displacement in x- and y-directions are solved independently. Thus, no bending is allowed along the coarse cells edges. The reduced-dimensional condition described by Eq. (17) is solved algebraically. For this purpose, the fine-

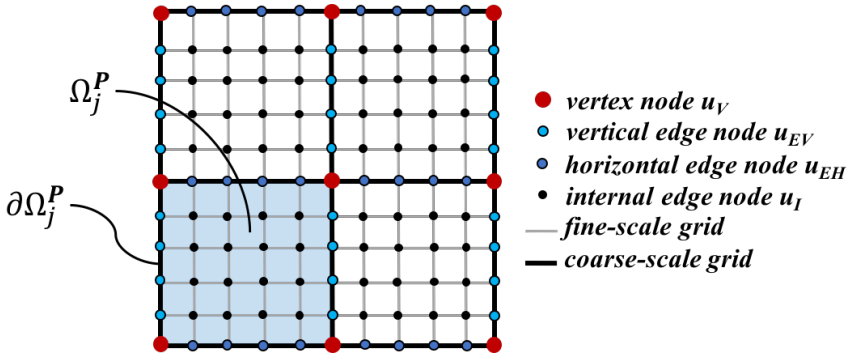

Figure 2: Primal coarse and fine-scale MSFV grids for mechanical deformation. $\Omega_j^\mathbf{P}$ denotes primal coarse block j and $\partial\Omega_j^\mathbf{P}$ corresponds to primal coarse cell boundary.

scale displacement nodes are classified as vertex, internal, horizontal and vertical edge nodes as shown in Fig. 2 [20]. Displacement solution at vertex nodes is obtained by solving coarse scale Eq. (12). Thus, the linear system for 2D mechanical deformation with reduced conditions along the coarse cells edges reads

$$\begin{bmatrix} A_{xx}^{II} & A_{xx}^{IEh} & A_{xx}^{IEv} & A_{xx}^{IV} & A_{xy}^{II} & A_{xy}^{IEh} & A_{xy}^{IEv} & A_{xy}^{IV} \\ 0 & A_{\parallel xx}^{EhEh} & 0 & A_{\parallel xx}^{EhV} & 0 & 0 & 0 & 0 \\ 0 & 0 & A_{\parallel yy}^{EvEv} & A_{\parallel yy}^{EvV} & 0 & 0 & 0 & 0 \\ 0 & 0 & 0 & (A_c)_{xx} & 0 & 0 & 0 & (A_c)_{xy} \\ A_{yx}^{II} & A_{yx}^{IEh} & A_{yx}^{IEv} & A_{yx}^{Ih} & A_{yy}^{II} & A_{yy}^{IEh} & A_{yy}^{IEv} & A_{yy}^{IV} \\ 0 & 0 & 0 & 0 & A_{\parallel xx}^{EhEh} & 0 & A_{\parallel xx}^{EhV} & 0 \\ 0 & 0 & 0 & 0 & 0 & 0 & A_{\parallel yy}^{EvEv} & A_{\parallel yy}^{EvV} \\ 0 & 0 & 0 & (A_c)_{yx} & 0 & 0 & 0 & (A_c)_{yy} \end{bmatrix} \cdot \begin{bmatrix} u_x'^I \\ u_x'^{Eh} \\ u_x'^{Ev} \\ u_x'^V \\ u_y'^I \\ u_y'^{Eh} \\ u_y'^{Ev} \\ u_y'^V \end{bmatrix} = \begin{bmatrix} 0 \\ 0 \\ 0 \\ (F_c)_{u_{cx}} \\ 0 \\ 0 \\ 0 \\ (F_c)_{u_{cy}} \end{bmatrix}, \tag{18}$$

where A_{ij} are sub-matrices stating the connectivities between unknowns u_i and u_j [20, 43]. Here superscripts I, Eh, Ev, V stand for internal, horizontal and vertical edge nodes and vertex nodes, respectively, whereas $((F_c)_{u_{cx}}, (F_c)_{uT_{cy}})^T = \mathbf{R_u}\bar{F}_u$. Consequently, prolongation operator $\mathbf{P_u}$ is obtained by writing displacement at internal and edge nodes in terms of the known displacement at vertex nodes (coarse solution).

With this approach, the resulting prolongation operator has a block structure, associated with $x-$ and $y-$ displacement components, as well as xy and yx cross terms, i.e.,

$$\mathbf{P_u} = \begin{bmatrix} {\mathbf{P_u}}^{xx} & {\mathbf{P_u}}^{xy} \\ {\mathbf{P_u}}^{yx} & {\mathbf{P_u}}^{yy} \end{bmatrix}. \tag{19}$$

Thus, the approximate fine-scale displacement solution is obtained, taking the interconnection of $x-$ and $y-$ displacement into account as

$$\begin{bmatrix} \bar{u}'_x \\ \bar{u}'_y \end{bmatrix} = \begin{bmatrix} \mathbf{P_u}^{xx} & \mathbf{P_u}^{xy} \\ \mathbf{P_u}^{yx} & \mathbf{P_u}^{yy}. \end{bmatrix} \cdot \begin{bmatrix} \bar{u}_{cx} \\ \bar{u}_{cy} \end{bmatrix}. \tag{20}$$

An example of basis functions for homogeneous and heterogeneous cases is illustrated in Fig. 3.

The restriction operator for displacement applies the same finite-volume integration in x- and y-directions over displacement coarse-scale control volumes. As such it has a block-diagonal structure with the same entries in each sub-block matrix, i.e.,

$$\mathbf{R_u} = \begin{bmatrix} \mathbf{R_u^{FV}} & 0 \\ \mathbf{0} & \mathbf{R_u^{FV}} \end{bmatrix}, \tag{21}$$

where the sub-block matrix $\mathbf{R_u^{FV}}$ have non-zero entries $r_{ij} = 1$ only if the fine-cell j belongs to the coarse grid cell i.

4.3. Construction of basis functions for flow

Multiscale formulation for flow constructs basis functions $\Phi_\mathbf{p}$ which are solved over dual coarse grids as shown in Fig. 4, i.e.,

$$p' = \mathbf{P_p} p_c, \tag{22}$$

where $\mathbf{P_p} = [\Phi_\mathbf{p}^1, ..., \Phi_\mathbf{p}^{N_\mathbf{p}^H}]$. Here, $N_\mathbf{p}^H$ is the number of coarse-scale pressure elements. The basis functions are obtained by solving the (flow-only) local mass balance equation, i.e.,

$$\begin{cases} -\boldsymbol{\nabla} \cdot \left(\lambda \cdot \boldsymbol{\nabla} {\Phi_\mathbf{p}}_j^i\right) = 0 & \text{in } \Omega_j^D \\ -\boldsymbol{\nabla}_\parallel \cdot (\lambda \cdot \boldsymbol{\nabla}_\parallel {\Phi_\mathbf{p}}_j^i) = 0 & \text{in } \partial\Omega_j^D \\ {\Phi_\mathbf{p}}_j^i(\bar{x}_k) = \delta_{ik} & \forall\ \bar{x}_k \in \{1, ..., N_\mathbf{p}^H\}, \end{cases} \tag{23}$$

where ${\Phi_\mathbf{p}}_j^i$ stands for a basis function associated with node i in dual coarse block Ω_j^D, subscript $\parallel$ denotes a reduced problem along primal coarse cell boundary $\partial\Omega_j^D$ and δ_{ik} is the Kronecker delta. A detailed description of algebraic procedure for flow basis function calculation is presented in the literature [20].

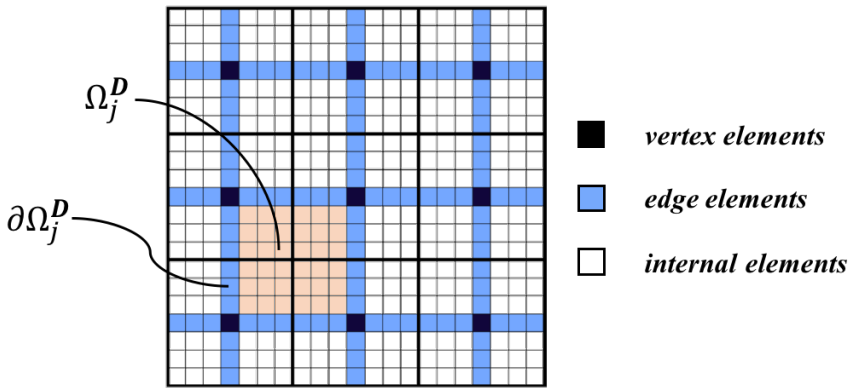

Figure 4: Dual coarse and fine-scale MSFV grids for flow. Ω_j^D denotes dual coarse block j and $\partial\Omega_j^D$ corresponds to dual coarse cell boundary.

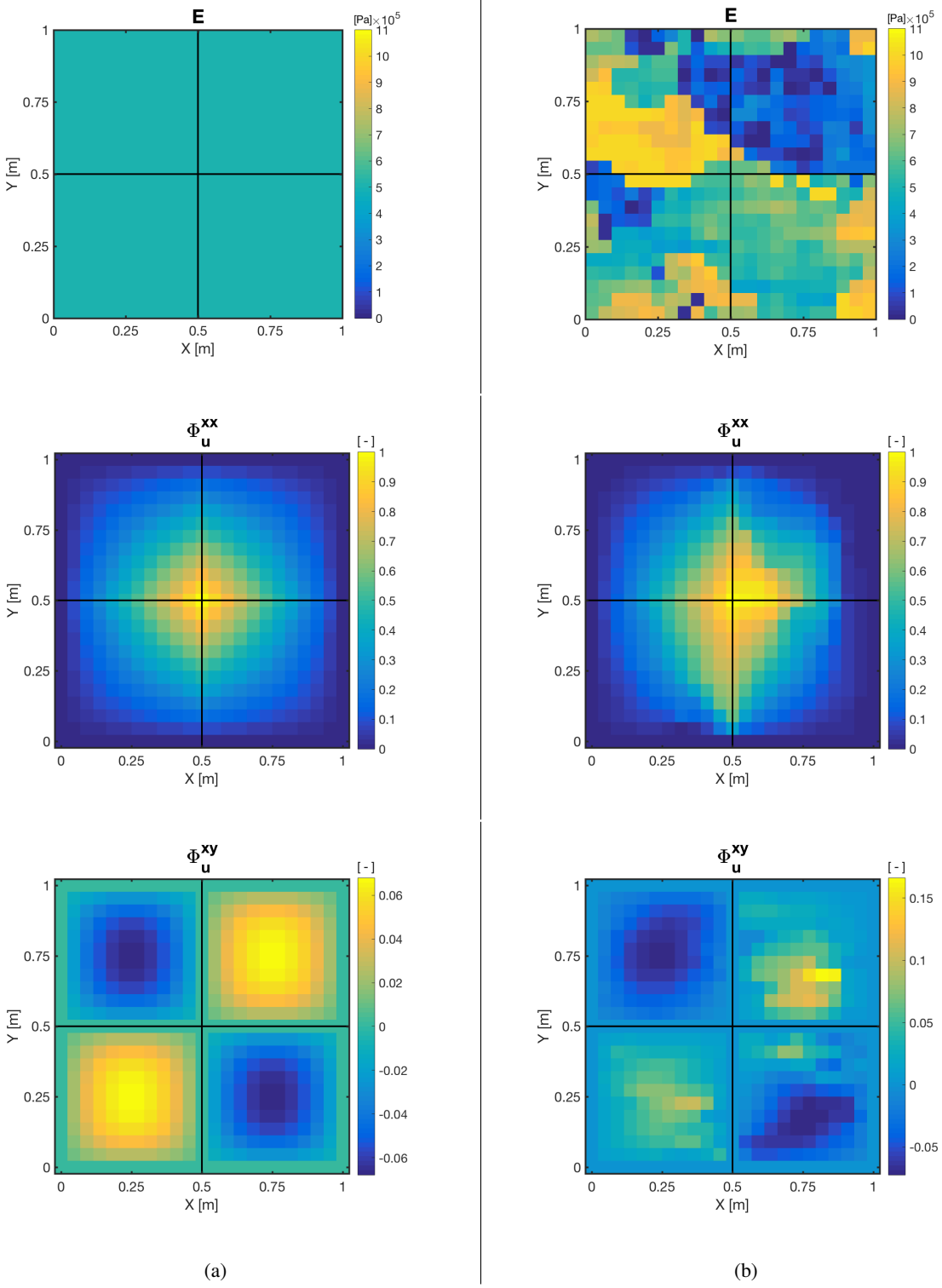

Figure 3: Example of basis functions for mechanical deformation in homogeneous (i.e., Fig. 3a) and heterogeneous (i.e., Fig. 3b) cases. Here the domain of $1 \times 1m^2$ is discretised by 22×22 fine and 2×2 coarse-scale displacement elements, respectively (coarse grid is denoted by solid black line). The upper row panels show Young's modulus distribution within the domain, the middle row depicts the basis function $\Phi_{\mathbf{u}}{}^{\mathbf{xx}}$ and the bottom row demonstrates the cross term $\Phi_{\mathbf{u}}{}^{\mathbf{xy}}$ of the basis function.

5. Numerical results

In this section several numerical examples, including benchmarking ones, are considered to investigate the developed methods. First, the consistency of the fine-scale FV discretization scheme is investigated for mechanical deformation on a synthetic test case, for which the analytical solution is known. Then, the fully implicit FV method is studied on Terzaghi (1D) and Mandel (2D) benchmarking test cases [1]. For Mandel test case, the order of consistency of the time-dependent pressure solution is presented. The accuracy of fully implicit MSFV method is investigated for both Terzaghi and Mandel test cases. For the latter, the MSFV results are compared with the hybrid Multiscale Finite Element-Finite Volume (h-MSFE-FV) method, which is recently developed by Castelletto et al. [39]. The applicability of the MSFV method to practical problems of reservoir simulation is shown for two heterogeneous test cases of simulating compaction process and land subsidence induced by reservoir depletion. Note that since the poroelasticity equations are linear, one can conveniently scale our synthetically selected K and E values with the factors α and β, respectively, i.e., $\tilde{K} = \alpha K$ and $\tilde{E} = \beta E$, in order to adjust them for a given realistic scenario. Doing so will scale other parameters as $\tilde{t} = t/\alpha$, $\tilde{\bar{u}} = \bar{u}/\beta$, $\tilde{M}_b = \beta M_b$, $\tilde{\lambda} = \alpha\lambda/\beta$ and $\tilde{q} = \alpha q/\beta$.

5.1. Synthetic test case for mechanical equilibrium

Consistency of fine-scale FV scheme for mechanical equilibrium is illustrated on a synthetic test case with known analytical solution. A set of exact solutions for x- and y-displacement is defined as

$$\begin{aligned} u_x &= 10^{-5} \sin\left(\frac{\pi x}{L}\right) \sin\left(\frac{\pi y}{W}\right) \\ u_y &= 10^{-5} \cos\left(\frac{\pi (L-x)}{L}\right) \sin\left(\frac{\pi y}{W}\right), \end{aligned} \tag{24}$$

where L and W are domain length and width respectively. Internal forces that would cause this solution are obtained analytically and used as source terms in the numerical simulation. For this test case, a homogeneous medium is considered with dimensions $L = W = 10$ m, the elastic moduli are $E = 4 \cdot 10^8$ Pa and $\nu = 0.33$. Dirichlet boundary conditions are applied at all four domain boundaries. Everywhere in the manuscript, except mentioned otherwise, the error is calculated based on scaled-L^∞ norm defined as

$$\varepsilon = \frac{\left\| \mathbf{x}_{ref} - \mathbf{x}' \right\|_\infty}{\left\| \mathbf{x}^h_{ref} \right\|_\infty} = \frac{\max_{i \in \{1,2,\ldots,N^h\}} \left| \mathbf{x}_{ref,i} - \mathbf{x}'_i \right|}{\max_{i \in \{1,2,\ldots,N^h\}} \left| \mathbf{x}_{ref,i} \right|}, \tag{25}$$

where N^h is the total number of the elements and $\mathbf{x}' = \bar{u}'$ or $\mathbf{x}' = p'$ for estimating displacement or pressure errors, respectively. Either analytical solution or fully resolved fine-scale solutions can be considered as a reference.

The convergence test is performed by refining the grid from 10×10 fine-scale grid cells to 100×100 with the step of 10 cells. The error plot, as shown in Fig. 5, illustrates that the introduced FV discretisation scheme is 2nd order accurate in space.

5.2. Terzaghi problem

Fine-scale and Multiscale FV methods are validated for the Terzaghi test case in a 1D domain [1]. This test case describes a fluid-saturated column of height L with a constant loading applied from the top. Drainage is allowed through the upper moving boundary only, whereas the column base is fixed. The load is applied instantaneously at time $t = 0$ yielding a non-zero initial overpressure and a corresponding displacement. The model parameters are as follows. The column length and the Young's modulus are $L = 1$ m and $E = 10^4$ Pa, respectively. Also, the Poisson's ratio is $\nu = 0.2$ and Biot's modulus is $M = 10^{100}$ Pa in order to simulate incompressible fluid and grains. Rock permeability is $K = 10^{-7}$ m^2 and fluid viscosity $\mu_f = 10^{-3}$ Pa $\cdot$ s. In addition, the Biot's coefficient of $b = 1$ is employed, which corresponds to strongly coupled (flow-mechanics) system. Constant load at the top boundary is 100 Pa.

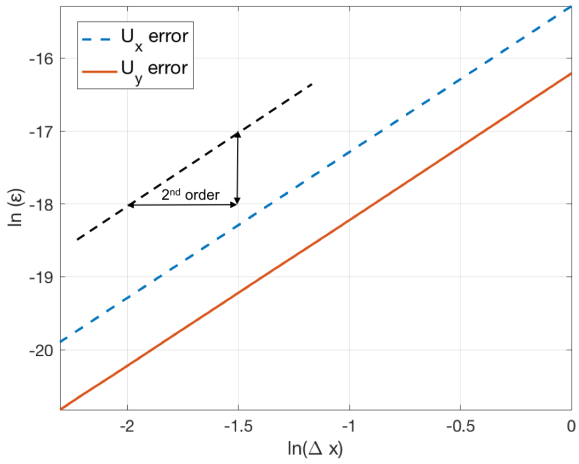

Figure 5: Error plot for synthetic test case for mechanical equilibrium. The solution for x- and y- displacement is 2nd order consistent in space.

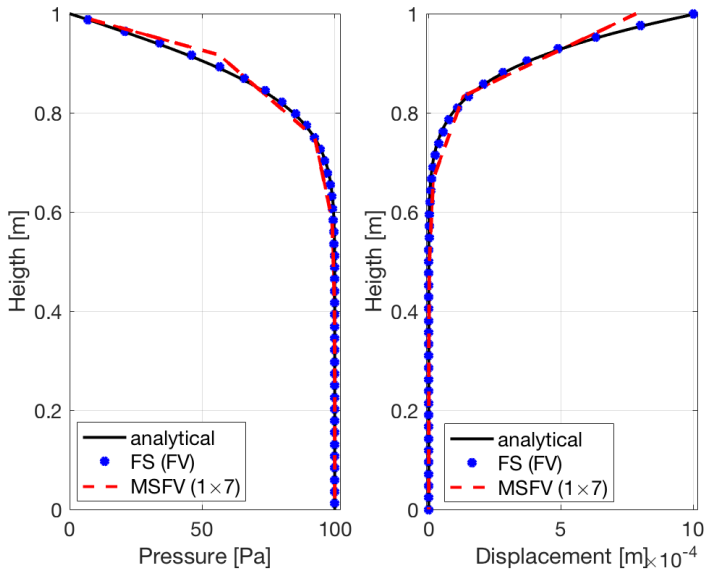

Figure 6: Terzaghi problem: the left figure corresponds to vertical pressure distribution in fluid saturated column; the right figure represents displacement distribution along the column. Analytical solution is denoted by solid black line; dotted blue line corresponds to fine-scale solution with 42 pressure and 42 displacement elements, red dashed line represents multiscale solution obtained with coarsening ratio of 7 for all unknowns. Analytical, fine-scale and multiscale solutions are obtained with constant time step $\Delta t = 0.0009$ s, and compared at $t = 0.009$ s.

Computational domain entails 42 pressure and 42 displacement elements at fine scale, which grid size of $\Delta x = 0.024$ m. For multiscale solution, the same coarsening ratio is applied to both pressure and displacement unknowns.

The quality of the multiscale solution $\mathbf{x}'$ is accessed individually for pressure and displacement with respect to the reference solution $\mathbf{x}_{ref}$ in terms of the scaled L^∞-norm as stated in Eq. (25).

Table 1: Terzaghi test case: accuracy of mutiscale solution for pressure and displacement obtained with different coarsening ratios. Here $\varepsilon_{\mathbf{p}}$ and $\varepsilon_{\mathbf{u}}$ stand for errors of approximate pressure and displacement solutions respectively. Pseudo-1D fine-scale grid consists of 42 pressure and displacement elements. The error of multiscale solution is reported for coarsening ratios of 3 and 7.

Coarsening ratio (# of fine elements per coarse)	$\varepsilon_{\mathbf{u}}$	$\varepsilon_{\mathbf{p}}$
3	3.61×10^{-2}	3.33×10^{-2}
7	1.23×10^{-1}	1.19×10^{-1}

Fig. 6 shows a snapshot of pressure and displacement profiles at early time after the loading is applied; thus, the fastest pressure change happens in a proximity of the upper boundary. The fine-scale solution accurately represents pressure and displacement fields, as shown in Fig. 6. The biggest error is observed for displacement at the upper boundary, caused by the finite volume restriction operator for displacement with no correction nor iterative improvement strategy. This restriction operator, however, guarantees the conservation of stress and mass at coarse scale. Overall, the accuracy of the multiscale results are quite satisfactory. The error of MSFV method is reported in table 1.

5.3. Mandel problem

Mandel problem is a classical benchmarking case for linear elastic poromechanics, in which a non-monotonic pressure behaviour is observed [1]. The problem describes an infinitely long homogeneous poroelastic slab saturated with fluid and bounded by two rigid, frictionless and impermeable plates. A constant load is applied instantaneously from the top at t = 0 yielding a non-zero initial overpressure and a corresponding displacement. Drainage is allowed from the side boundaries of the slab.

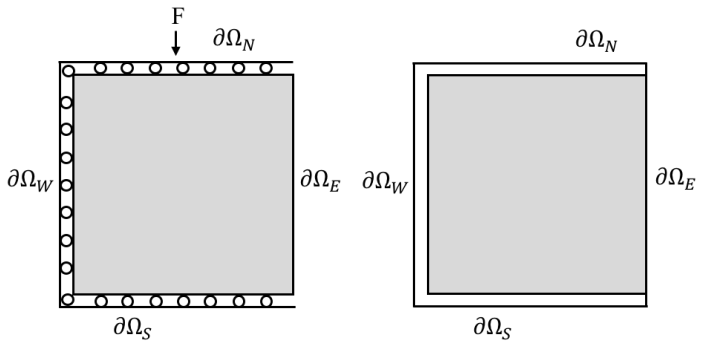

Figure 7: Mandel problem set-up for mechanical deformation (i.e., Fig. 7a) and flow (i.e., Fig. 7b). The domain is subject to roller constrain at south, west and north boundaries, whereas the east boundary is considered traction-free. No-flow boundary conditions are imposed at south, west and north boundaries, whereas the drainage is allowed through the east boundary.

Taking the advantage of its symmetric geometry, as shown in Fig. 7, the computational domain is considered for the top-right quarter of the shown physical domain with appropriate symmetry boundary conditions applied at the west and the south boundaries. At the north boundary, the prescribed y-displacement resulting from the applied loading is imposed. Thus, the boundary conditions of 2D Mandel problem read

$$-(\lambda \cdot \boldsymbol{\nabla} p) \cdot \bar{n} = 0, \quad u_x = 0, \quad \sigma_{xy} = 0 \quad (x, y) \in \partial\Omega_W \tag{26a}$$

$$p = 0, \quad \sigma_{xx} = 0, \quad \sigma_{xy} = 0 \quad (x, y) \in \partial\Omega_E \tag{26b}$$

$$-(\lambda \cdot \boldsymbol{\nabla} p) \cdot \bar{n} = 0, \quad u_y = 0, \quad \sigma_{xy} = 0 \quad (x, y) \in \partial\Omega_S \tag{26c}$$

$$-(\lambda \cdot \boldsymbol{\nabla} p) \cdot \bar{n} = 0, \quad u_y = u^* \quad \sigma_{xy} = 0 \quad (x, y) \in \partial\Omega_N \tag{26d}$$

Here, u^* is taken from the analytical solution to the Mandel problem [1]. We consider computational domain of 1×1 m with the following model parameters: Young's modulus $E = 10^4$ Pa, Poisson's ratio $\nu = 0.2$ and Biot's modulus $M = 10^{100}$ in order to simulate incompressible fluid and grains. Rock permeability is $K = 10^{-7}$ m^2 and fluid viscosity $\mu_f = 10^{-3}$ Pa $\cdot$ s. Moreover, the Biot's coefficient of $b = 1$ is employed, which corresponds to strongly coupled (flow-mechanics) system. These parameters result in characteristic consolidation time $t = 0.9$ s, which is considered as end of the simulation. Constant load at the top boundary is 2 Pa. The above mentioned model parameters are used in simulations for fine-scale and multiscale FV methods validation, described in the following sections.

5.3.1. Fully coupled fine-scale FV method validation

The proposed fine-scale fully coupled FV method is validated on benchmarking Mandel test case. Moreover, the results are compared with the fine-scale hybrid finite element-finite volume (h-FE-FV) scheme, where mechanical deformation is solved using FE discretization, whereas flow is solved based on FV method.

Figure 8a shows a change of pressure at central point of the domain (which is equidistant from all four boundaries) over time. Here computational domain entails 99×99 pressure and displacement elements at fine scale, with a grid size of $\Delta x = \Delta y = 0.0101$ m, whereas the time step of simulation is $\Delta t = 0.003$ s. Note that the fine-scale solution accurately captures non-linear pressure behaviour. Moreover, the results obtained with fine-scale discrete FV and h-FE-FV methods are close. Note that FV scheme produces conservative stress field.

With this numerical example we demonstrate the consistency of time-dependent pressure solution. The error map shown in Fig. 8b was obtained by estimating the error of numerical pressure solution at the central point of the domain at the end of the simulation with a range of time steps between 0.018 s and 0.0018 s and grid sizes between 0.1 m and 0.01 m. The resulting error plot, presented in Fig. 8b, shows that, as expected, pressure solution is 1st order accurate in time, while the order of accuracy for both unknowns in space is 2 (shown in section 5.1).

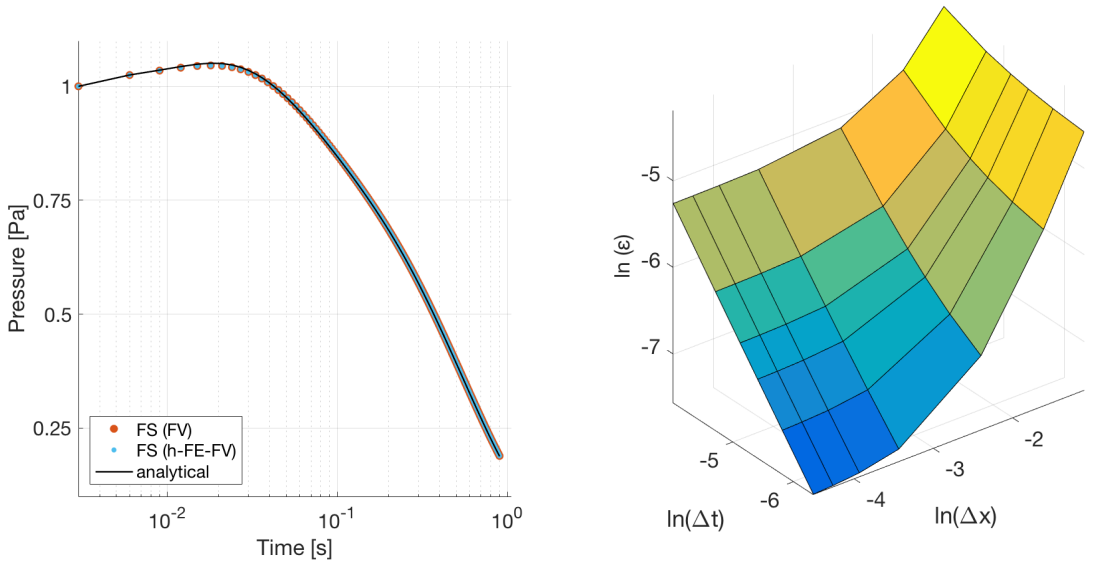

(a) (b)

Figure 8: Fine-scale simulation results for Mandel's problem. Fig. 8a depicts pressure history at central point of the domain over time. The fine-scale mesh consists of 99×99 pressure and displacement elements, whereas the time step $\Delta t = 0.003$ s. The results obtained with fully coupled FV and h-FE-FV methods are shown for comparison. Fig. 8b shows error map for time-dependent pressure solution obtained with fully coupled FV method.

5.3.2. MultiScale solution

The proposed MSFV method is validated on Mandel test case with model parameters described in Section 5.3. Moreover, MSFV results are compared with a solutions obtained with h-MSFE-FV method for a series of coarsening

ratios. Similar to Section 5.3.1, computational domain entails 99×99 pressure and displacement elements at fine scale, with a grid size of $\Delta x = \Delta y = 0.0101$ m, whereas the time step of simulation is $\Delta t = 0.003$ s.

Fig. 9 shows pressure history at central point of the domain over time, reconstructed from coarse-scale solutions obtained with different coarsening factors. The results of MSFV method and h-MSFE-FV method are shown in Fig. 9a and Fig. 9b, respectively, for comparison. Although the performance of both methods for coarsening ratios of 11×11 and 3×3 are similar, the result of MSFV method with the most aggressive coarsening ratio (i.e., 33×33) is significantly more accurate. This effect is especially visible at the beginning of simulation where most of the non-linear pressure behaviour is observed. Presumably, lack of stress conservation produced by h-MSFE-FV method has an influence on pressure solution over the larger coarse cells, whereas MSFV method remains stable even for the extreme coarsening ratios.

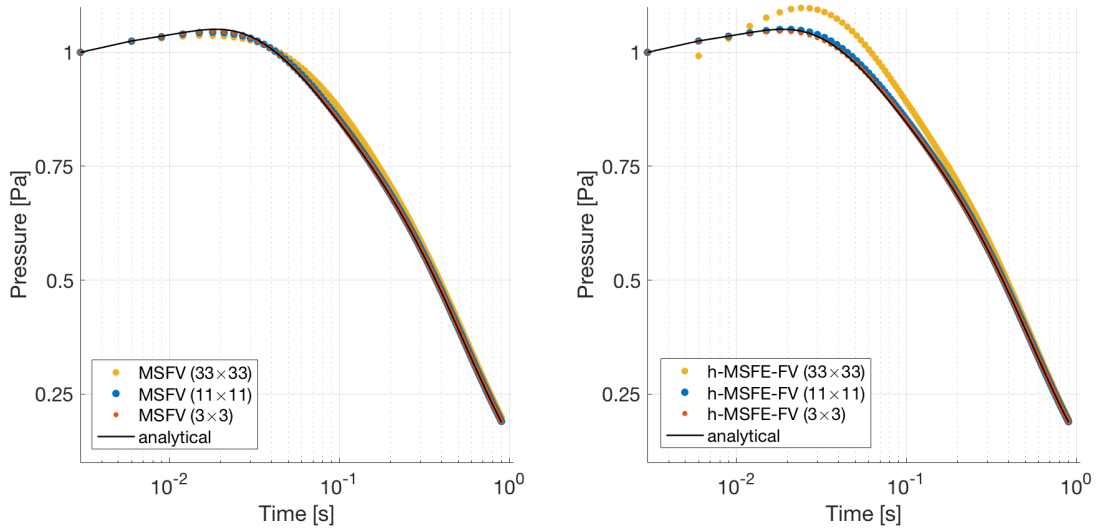

(a) (b)

Figure 9: Pressure history at central point of the domain over time, reconstructed from coarse-scale solutions obtained with different coarsening ratios (denoted in legend in parenthesis). Figures 9a and 9b show the results of MSFV and h-MSFE-FV methods respectively. Computational domain entails 99×99 pressure and displacement elements at fine scale. Multiscale solutions are presented for coarsening ratios of 33×33, 11×11 and 3×3 fine elements per coarse.

The accuracy of MSFV method is accessed by estimating the error of pressure and displacement solutions with regards to analytical solution as shown in Eq. (25). The error is calculated in the end of simulation for a series of numerical experiments performed with different coarsening ratios. The detailed error report is presented in table 2. Note that the MSFV method provides conservative solutions for both pressure and displacement with accuracy comparable to h-MSFE-FV method.

5.4. Plain strain subsidence

Modelling of land subsidence induced by reservoir depletion is a practical problem for geo-engineering applications. In this numerical experiment, we consider the subsurface as a heterogeneous porous medium, where the elastic properties vary in z-direction. Based on this assumption, a 3D problem can be reduced to 2D under plain strain conditions. This study is focused on modelling of mechanical deformation response on a complete depletion of the reservoir, thus, the dynamics of fluid flow within the reservoir is not simulated.

The producing reservoir is 120 m thick and 1200 m wide. Reservoir top is located at the depth of 1000 m. Mechanical deformation is modelled within the span of 10 km in x-direction and 3 km in y-direction. Initial reservoir pressure of 100 bar corresponds to normally pressurised formation at the depth of consideration, assuming normal fluid gradient of 0.1 bar/m. The distribution of Young's modulus in the subsurface is obtained based on a constitutive

Table 2: Mandel test case: accuracy of MSFV and h-MSFE-FV methods for different coarsening ratios; $\varepsilon_{\mathbf{p}}$ and $\varepsilon_{\mathbf{u}}$ stand for errors of approximate pressure and displacement solutions respectively. The fine-scale grid consists of 99×99 pressure and displacement elements. The error of multiscale solution is presented for coarsening ratios of 33×33, 11×11, 9×9 and 3×3 fine elements per coarse.

Coarsening ratio	MSFV		h-MSFV-FE	
(# of fine elements per coarse)	$\varepsilon_{\mathbf{p}}$	$\varepsilon_{\mathbf{u}}$	$\varepsilon_{\mathbf{p}}$	$\varepsilon_{\mathbf{u}}$
33×33	3.90×10^{-2}	1.61×10^{-2}	1.91×10^{-2}	6.21×10^{-3}
11×11	8.43×10^{-3}	3.18×10^{-3}	5.98×10^{-3}	9.87×10^{-4}
9×9	7.15×10^{-3}	2.66×10^{-3}	5.49×10^{-3}	1.17×10^{-3}
3×3	4.83×10^{-3}	1.73×10^{-3}	4.66×10^{-3}	1.58×10^{-3}

model for one-dimensional vertical compressibility, developed in [42] for the northern Adriatic sedimentary basin. In this model, the vertical uniaxial compressibility c_M is related to vertical effective stress σ'_y as

$$c_M = 0.01241 \left|\sigma'_y\right|^{-1.1342}, \tag{27}$$

where c_M and σ'_y are expressed in [bar^{-1}] and [bar] respectively and the vertical effective stress is obtained as superposition of total vertical stress σ_y and hydrostatic pressure p, i.e.,

$$\sigma'_y = \sigma_y + p = \underbrace{-0.12218\,|y|^{1.0766}}_{\sigma_y} + \underbrace{0.1\,|y|}_{p}. \tag{28}$$

The Poisson ratio $\nu = 0.3$ is assumed for the whole section. Thus, Young's modulus can be expressed implicitly as a function of depth (see Fig. 10a) through c_M, i.e.,

$$E = \frac{(1-2\nu)(1+\nu)}{(1-\nu)c_M}. \tag{29}$$

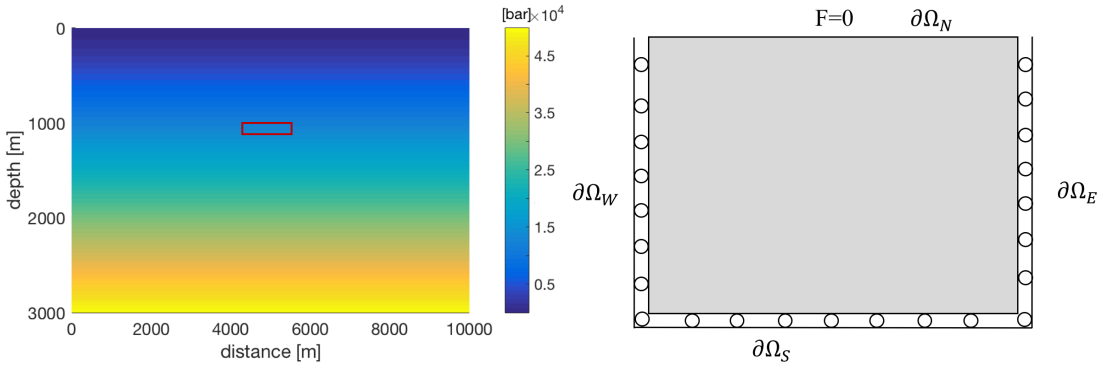

(a) (b)

Figure 10: Plain strain subsidence model. Figure 10a depicts Young's modulus distribution within geological section, described by Eq. (29). Location of the reservoir is denoted by the red box. Figure 10b illustrates boundary conditions for mechanical deformation: the domain is subject to roller constrains at west, east and south boundaries, whereas the north boundary is traction-free.

The domain is subject to roller constrains at west, east and south boundaries, whereas the north boundary is traction-free (Fig. 10b). Computational domain is discretised at fine scale by 450×225 elements, resulting in fine cell size of 22.2×13.3 m^2. In order to keep the system in equilibrium at initial reservoir conditions, the initial reservoir pressure is added as a source term for mechanical equilibrium in agreement with Eq. (1), where $f = 0$. Ultimately, the reservoir is considered to be fully depleted, thus, the overall pressure drop $\Delta p = 100$ bar.

The multiscale solution is obtained with coarsening ratio of 9×9 fine-scale displacement elements per coarse, resulting in 51×26 coarse displacement nodes against 451×226 nodes on the fine-scale. Fig. 11 shows the comparison of the reference fine-scale and multiscale solutions. The error of land subsidence estimation is accessed relative to the fully resolved fine-scale solution as shown in Eq. (25).

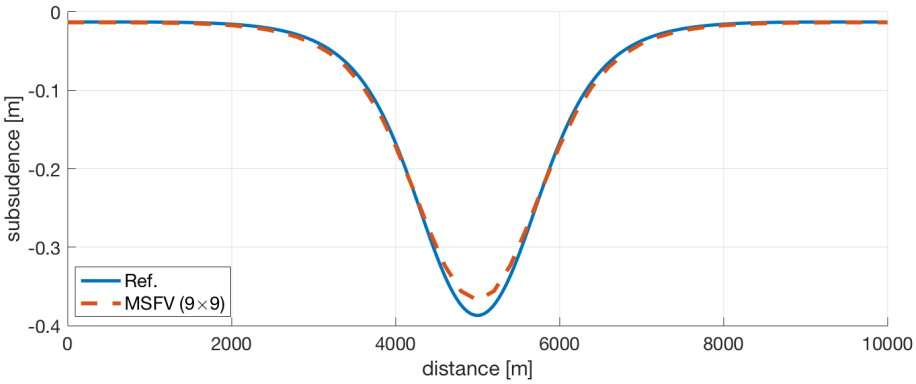

Figure 11: Plain strain subsidence test case: comparison of multiscale solution obtained with MSFV method (dashed red line) and reference fine-scale (FV) solution (solid blue line). The fine-scale grid consists of 450×225 displacement elements, whereas the MSFV coarse-scale mesh conatins 50×25 elements.

For the chosen coarsening ratio, mean error does not exceed 5.3% as shown in table 3. Overall, the quality of multiscale solution is satisfactory.

Table 3: Plain strain subsudence: accuracy of mutiscale solution for displacement obtained with 9×9 coarsening ratio; $\varepsilon_{\mathbf{u}}$ stands for the displacement solution error. The fine-scale grid consists of 450×225 displacement elements. The error of multiscale solution is presented for coarse mesh with 50×25 coarse elements.

Coarsening ratio (# of fine elements per coarse)	$\varepsilon_{\mathbf{u}}$
9×9	5.26×10^{-2}

5.5. Compaction of heterogeneous media

This test case is inspired by classical Terzaghi problem described in section 5.2. In this numerical example, a compaction process of 2D heterogeneous medium is modelled. The aim of this numerical experiment is to test the ability of MSFV method to capture heterogeneities.

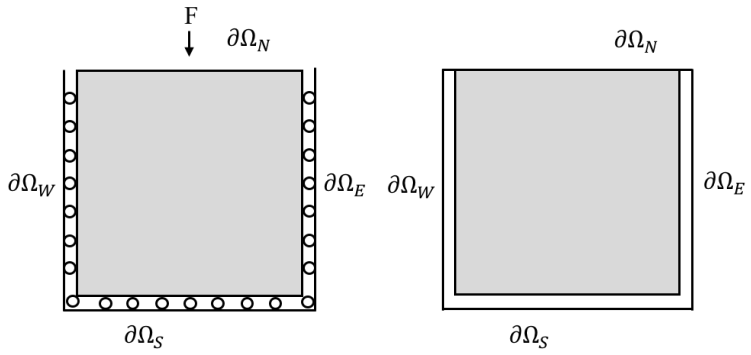

Figure 12: A set-up for compaction of a heterogeneous medium test case. Fig. 12a and 12b illustrate boundary conditions for mechanical deformation and flow respectively. The domain is subject to roller constrain at south, west and east boundaries, whereas the constant vertical loading is applied at the northern boundary. No-flow boundary conditions are imposed at south, west and east boundaries, whereas the drainage is allowed through the north boundary.

We consider a fluid-saturated domain of 1×1 m^2 with highly heterogeneous mechanical and hydraulic properties, originally taken from a part of SPE10 dataset and scaled to derive elastic and hydraulic properties. The constant Piossin's ratio of $\nu = 0.2$ is considered for the entire domain. A constant loading of 100 Pa is applied at the top. The initial fluid pressure of 100 Pa is uniformly distributed throughout the domain. The applied vertical loading results in compaction of the domain, whereas saturating fluid is allowed to drain through the northern boundary. Fine-scale mesh entails 45×45 pressure and displacement elements. As illustrated in Fig. 12, the domain is subject to roller constrains at all boundaries except north, where the constant loading is applied. All the boundaries except north are subject to no-flow boundary conditions, whereas zero pressure is considered at the north. The resulting deformation and pressure are obtained at $t = 0.06$ s with the time step $\Delta t = 2 \times 10^{-4}$ s.

In section 5.3.2 it is shown that reducing coarsening ratio leads to the reduction of error for homogeneous media. However, that is not always the case if there are heterogeneities involved. Thus, the quality of multiscale solution is accessed for a series of experiments with varying coarsening ratios. The detailed error report is presented in table 4. As Fig. 13 shows, the MSFV solution obtained with very high coarsening factor of 15×15 can be considered a valid approximation of the reference fine-scale (FV) solution for both pressure and displacement. The error of MSFV solution (see table 4) for displacement varies from 7% to 21%, whereas the error of pressure solution lies in the range between 2% and 14%.

Table 4: Compaction of heterogeneous media test case: accuracy of multiscale (MSFV) solution for displacement and pressure, obtained with various coarsening factors; $\varepsilon_{\mathbf{u}}$ and $\varepsilon_{\mathbf{p}}$ correspond to the errors of displacement and pressure solutions with respect to reference fine-scale (FV) solution. The fine-scale grid consists of 45×45 pressure and displacement elements. The errors are reported for a series of multiscale solutions obtained with coarsening ratios from 15×15 to 3×3 at $t = 0.06$ s with the time step $\Delta t = 2 \times 10^{-4}$ s.

Coarsening ratio (# of fine elements per coarse)	$\varepsilon_{\mathbf{u}}$	$\varepsilon_{\mathbf{p}}$
3×3	1.15×10^{-1}	1.88×10^{-2}
5×5	6.88×10^{-2}	4.54×10^{-2}
9×9	1.39×10^{-1}	5.97×10^{-2}
15×15	2.10×10^{-1}	1.42×10^{-1}

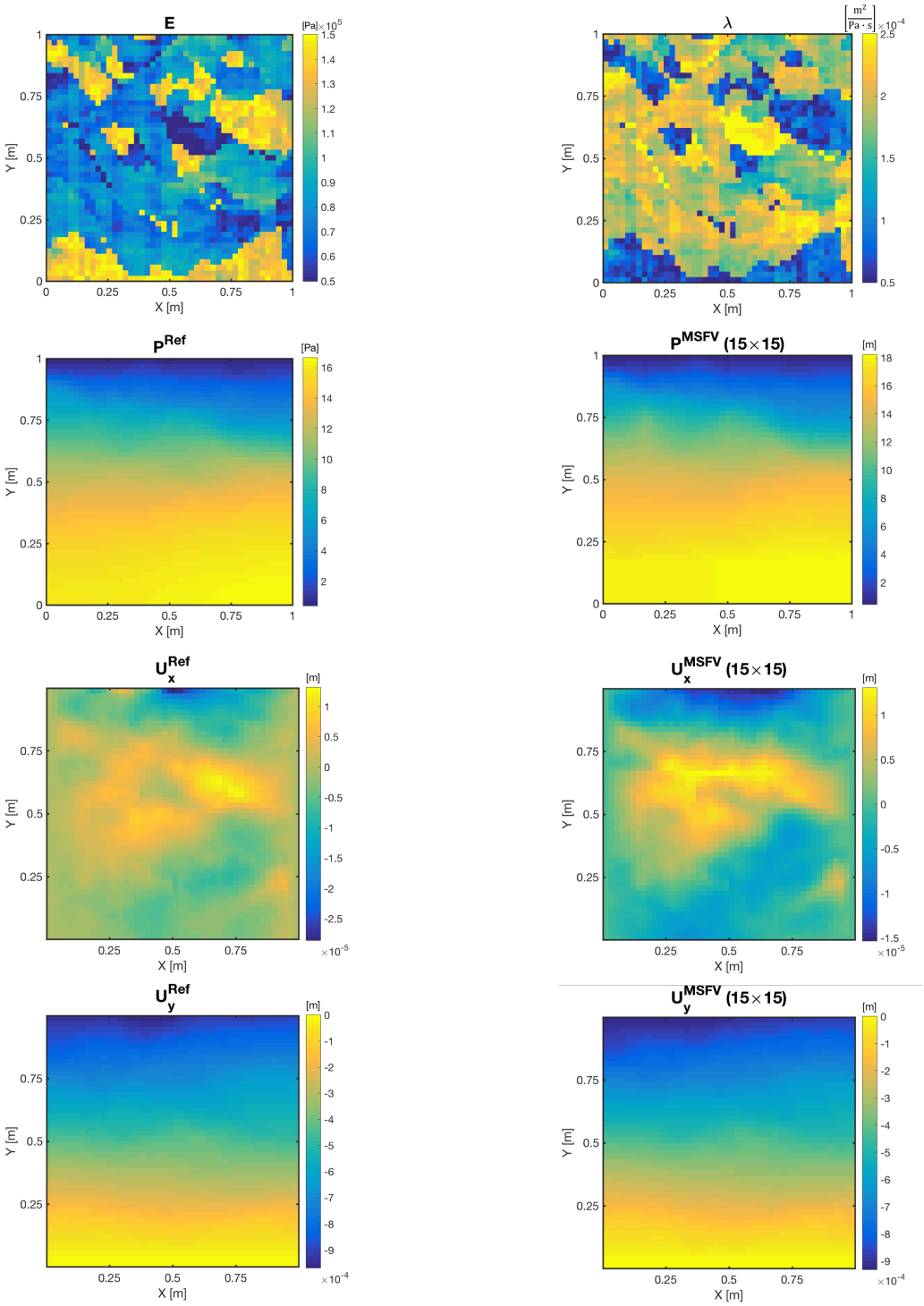

Figure 13: Simulation results for compaction of heterogeneous media test case. The upper row illustrates elastic (Young's modulus E) and hydraulic (fluid mobility λ) properties on the left and right figures respectively. Rows 2-4 show the comparison of the reference fine-scale (FV) solution for pressure, x- and y-displacement (figures on the left) with the corresponding multiscale solutions obtained with MSFV method (figures on the right). Fine-scale mesh entails 45×45 pressure and displacement elements, whereas the coarsening factor for multiscale solution is 15×15. The end time of simulation is $t = 0.06$ s and the time step $\Delta t = 2 \times 10^{-4}$ s.

6. Conclusions

In this work, a fully implicit Multiscale finite volume method (MSFV) for fully-coupled flow-mechanics simulations under linear elasticity is proposed. Finite volume discretisation for both flow and deformation is motivated by conservative nature of mass and momentum balance equations. In finite volume (FV) discretisation scheme for mechanical deformation, displacement derivatives are approximated based on bilinear interpolation functions. FV discretisation of mechanical deformation is integrated into fully coupled fully implicit poromechanics simulation framework based on Biot's theory.

MSFV framework is built on the developed fully-implicit finite-volume-based fine-scale system. Independent coarse grids for flow and deformation are imposed on this fine-scale computational domain. Basis functions for pressure and displacement are computed algebraically by solving a set of local problems with reduced boundary conditions at the coarse volume boundaries. Note that our MSFV method constructs the basis functions at the beginning of the simulation, and for all the next time steps, it employs them (with no update) to construct and solve the coarse-scale system. As for the restriction, a FV-based operators was used in order to apply an integration over the coarse scale control volumes (for both displacement and pressure).

To verify the method, first the consistency of the fully-coupled fine-scale FV poromechanics discretisation scheme was investigated for Terzaghi and Mandel benchmarking problems. The accuracy of MSFV method was studied for the two aforementioned test cases and was also compared to h-MSFE-FV method. Moreover, MSFV method was tested on practical problems of reservoir simulation, involving land subsidence and modelling of heterogeneous rock compaction. Numerical results showed that the developed MSFV method provides an accurate approximation of the fine-scale results. Thus it casts a promising approach for simulation on large-scale heterogeneous fields. Similar to the flow [43], further research is required to benchmark the overall speed-up of the devised multiscale approach for coupled flow-deformation in 3D heterogeneous geoscience applications.

Acknowledgments

The authors thank Nicola Castelletto for fruitful discussions. This work was performed at Delft Advanced Reservoir Simulation (DARSim) research group.

References

[1] H. Wang. *Theory of Linear Poroelasticity*. Princeton University Press, Princeton, NJ, 2000.
[2] K. Aziz and A. Settari. *Petroleum Reservoir Simulation*. Applied Science Publishers, 1979.
[3] T. J. R. Hughes. *The Finite Element Method: Linear Static and Dynamic Finite Element Analysis*. Dover Publications, 2000.
[4] T. Arbogast, M. F. Wheeler, and I. Yotov. Mixed finite elements for elliptic problems with tensor coefficients as cell-centered finite differences. *SIAM J. Numer. Anal.*, 34:828–852, 1997.
[5] A. Masud and T. J. R. Hughes. A stabilized mixed finite element method for darcy flow. *Comput. Methods Appl. Mech. Eng.*, 191(39):4341 – 4370, 2002.
[6] K. Olesen, B. Gervang, J. N. Reddy, and M. Gerritsma. A higher-order equilibrium finite element method. *Int. J. Numer. Meth. Eng*, 114(12):1262–1290, 2018.
[7] F.J. Gaspar, F.J. Lisbona, and P.N. Vabishchevich. A finite difference analysis of biot's consolidation model. *Appl. Numer. Math.*, 44(4):487 – 506, 2003.
[8] F.J. Gaspar, F.J. Lisbona, and P.N. Vabishchevich. Staggered grid discretizations for the quasi-static biot's consolidation problem. *Appl. Numer. Math.*, 56(6):888 – 898, 2006.
[9] E. Ucar, E. Keilegavlen, I. Berre, and J. Nordbotten. A finite-volume discretization for deformation of fractured media. *Computat. Geosci.*, pages DOI: 10.1007/s10596–018–9734–8, 2018.
[10] R. Deb and P. Jenny. Finite volume-based modeling of flow-induced shear failure along fracture manifolds. *Int. J. Numer. Anal. Methods Geomech.*, 41(18):1922–1942, 2017.
[11] R. Deb and P. Jenny. Modeling of shear failure in fractured reservoirs with a porous matrix. *Computat. Geosci.*, 21(5):1119–1134, 2017.
[12] J. Kim, H. A. Tchelepi, and R. Juanes. Stability, accuracy, and efficiency of sequential methods for coupled flow and geomechanics. *SPE J.*, 16:249–262, 2011.
[13] M. Ferronato, N. Castelletto, and G. Gambolati. A fully coupled 3-d mixed finite element model of biot consolidation. *J. Comput. Phys.*, 229:4813–4830, 2010.
[14] N. Castelletto, J. A. White, and H. A. Tchelepi. Accuracy and convergence properties of the fixed-stress iterative solution of two-way coupled poromechanics. *International Journal for Numerical and Analytical Methods in Geomechanics*, 39(14):1593–1618, 2015.
[15] T. T. Garipov, M. Karimi-Fard, and H. A. Tchelepi. Discrete fracture model for coupled flow and geomechanics. *Computat. Geosci.*, 20(1):149–160, 2016.

[16] S. Dana and M. F. Wheeler. Convergence analysis of fixed stress split iterative scheme for anisotropic poroelasticity with tensor biot parameter. *Computat. Geosci.*, 2018.
[17] M. Borregales, F.A. Radu, K. Kumar, and J.M. Nordbotten. Robust iterative schemes for non-linear poromechanics. *Computational Geosciences*, 22:1021–1038, 2018.
[18] P. Jenny, S. H. Lee, and H. A. Tchelepi. Multi-scale finite-volume method for elliptic problems in subsurface flow simulation. *J. Comput. Phys.*, 187:47–67, 2003.
[19] H. Hajibeygi, G. Bonfigli, M. A. Hesse, and P. Jenny. Iterative multiscale finite-volume method. *J. Comput. Phys.*, 227(19):8604 – 8621, 2008.
[20] Y. Wang, H. Hajibeygi, and H. A. Tchelepi. Algebraic multiscale linear solver for heterogeneous elliptic problems. *J. Comput. Phys.*, 259:284–303, 2014.
[21] O. Møyner and K.A Lie. A multiscale restriction-smoothed basis method for high contrast porous media represented on unstructured grids. *J. Comput. Phys.*, 304:46–71, 2016.
[22] L. A. Caudillo-Mata, E. Haber, and C. Schwarzbach. An oversampling technique for the multiscale finite volume method to simulate electromagnetic responses in the frequency domain. *Computational Geosciences*, 21(5):963–980, 2017.
[23] R. D. Cook. *Finite Element Modeling for Stress Analysis*. John Wiley & Sons, Inc., New York, NY, USA, 1994.
[24] T. Y. Hou and X. H. Wu. A multiscale finite element method for elliptic problems in composite materials and porous media. *J. Comput. Phys.*, 134:169–189, 1997.
[25] Y. Efendiev, T. Hou, and V. Ginting. Multiscale finite element methods for nonlinear problems and their applications. *Comm. Math. Sci.*, 2(4):553–589, 2004.
[26] Y. Efendiev, V. Ginting, T. Hou, and R. Ewing. Accurate multiscale finite element methods for two-phase flow simulations. *J. Comput. Phys.*, 220:155–174, 2006.
[27] Y. Wang, H. Hajibeygi, and H. A. Tchelepi. Monotone multiscale finite volume method. *Comput. Geosci.*, 20:509–524, 2015.
[28] Y. Efendiev and T. Y. Hou. *Multiscale finite element methods: theory and applications*, volume 4. Springer Science & Business Media, 2009.
[29] M. Vasilyeva, E. T. Chung, Y. Efendiev, and J. Kim. Constrained energy minimization based upscaling for coupled flow and mechanics. *Journal of Computational Physics*, 376:660–674, 2019.
[30] E. T. Chung, Y. Efendiev, and G. Li. An adaptive gmsfem for high-contrast flow problems. *Journal of Computational Physics*, 273:54 – 76, 2014.
[31] J. Franc, L. Jeannin, G. Debenest, and R. Masson. Fv-mhmm method for reservoir modeling. *Computational Geosciences*, 21(5):895–908, Dec 2017.
[32] F. Furtado, V. Ginting, F. Pereira, and M. Presho. Operator splitting multiscale finite volume element method for two-phase flow with capillary pressure. *Transport in Porous Media*, 90(3):927–947, 2011.
[33] A. Kozlova, Z. Li, J.R. Natvig, S. Watanabe, Y. Zhou, K. Bratvedt, and S.H. Lee. A real-field multiscale black-oil reservoir simulator. *SPE J.*, 21:2049 – 2061, 2016.
[34] S. Shah, O. Møyner, M. Tene, K.A. Lie, and H. Hajibeygi. The multiscale restriction smoothed basis method for fractured porous media F-MsRSB. *J. Comput. Phys.*, 318:36–57, 2016.
[35] R. J. de Moraes, J. R.P. Rodrigues, H. Hajibeygi, and J.D. Jansen. Multiscale gradient computation for flow in heterogeneous porous media. *Journal of Computational Physics*, 336:644 – 663, 2017.
[36] M. Cusini, A. Lukyanov, J. Natvig, and H. Hajibeygi. Constrained pressure residual multiscale (cpr-ms) method for fully implicit simulation of multiphase flow in porous media. *J. Comput. Phys.*, 299:472–486, 2015.
[37] M. Cusini, C. van Kruijsdijk, and H. Hajibeygi. Algebraic dynamic multilevel (adm) method for fully implicit simulations of multiphase flow in porous media. *J. Comput. Phys.*, 314:60–79, 2016.
[38] M. HosseiniMehr, M. Cusini, C. Vuik, and H. Hajibeygi. Algebraic dynamic multilevel method for embedded discrete fracture model (f-adm). *Journal of Computational Physics*, 373:324 – 345, 2018.
[39] N. Castelletto, H. Hajibeygi, and H. A. Tchelepi. Hybrid multiscale formulation for coupled flow and geomechanics. *ECMOR XV, Amsterdam, Netherlands*, 2016.
[40] N. Castelletto, S. Klevtsov, H. Hajibeygi, and H. A. Tchelepi. Multiscale two-stage solver for biots poroelasticity equations in subsurface media. *Computational Geosciences*, 2019, https://doi.org/10.1007/s10596-018-9791-z.
[41] N. Castelletto, H. Hajibeygi, and H. A. Tchelepi. Multiscale finite-element method for linear elastic geomechanics. *J. Comput. Phys.*, 331:337 – 356, 2017.
[42] D. Baú, M. Ferronato, G. Gambolati, and P. Teatini. Basin-scale compressibility of the northern adriatic by the radioactive marker technique. *Géotechnique*, 52(8):605–616, 2002.
[43] M. Tene, M.S. Al Kobaisi, and H. Hajibeygi. Algebraic multiscale method for flow in heterogeneous porous media with embedded discrete fractures (f-ams). *J. Comput. Phys.*, 321:819 – 845, 2016.